Available online at www.sciencedirect.com
SCIENCE DIRECT®
Analytica Chimica Acta 496 (2003) 3–16
ANALYTICA CHIMICA ACTA
www.elsevier.com/locate/aca

Distance-dependent electron hopping conductivity and nanoscale lithography of chemically-linked gold monolayer protected cluster films

Francis P. Zamborini [a,*], Laura E. Smart [a], Michael C. Leopold [b,1], Royce W. Murray [b]

[a] *Department of Chemistry, University of Louisville, Louisville, KY 40292, USA*
[b] *Kenan Laboratories of Chemistry, University of North Carolina, Chapel Hill, NC 27599-3290, USA*

Received 25 October 2002; accepted 28 October 2002

Abstract

Films of monolayer protected Au clusters (MPCs) with mixed alkanethiolate and ω-carboxylate alkanethiolate monolayers, linked together by carboxylate–Cu^{2+}–carboxylate bridges, exhibit average edge-to-edge cluster spacings that vary with the numbers of methylene segments in the alkanethiolate ligand as determined by a combined atomic force microscopy (AFM)/UV-Vis spectroscopy method. The electronic conductivity (σ_{EL}) of dry films is exponentially dependent on the cluster spacing, consistent with electron tunneling through the alkanethiolate chains and non-bonded contacts between those chains on individual, adjacent MPCs. The calculated electronic coupling factor (β) for tunneling between MPCs is 1.2 $Å^{-1}$, which is similar to other values obtained for tunneling through hydrocarbon chains. Electron transfer rate constants measured on the films reflect the increased cluster–cluster tunneling distance with increasing chainlength. The MPC films are patterned by scanning the surface with an AFM or scanning tunneling microscopy (STM) tip under appropriate conditions. The patterning mechanism is physical in nature, where the tip scrapes away the film in the scanned region. Large forces are required to pattern films with AFM while normal imaging conditions are sufficient to produce patterns with STM. Patterns with dimensions as small as 100 nm are shown. Subsequent heating (300 °C) of the patterned surfaces leads to a metallic Au film that decreases in thickness and is smoother compared to the MPC film, but retains the initial shape and dimensions of the original pattern.

Keywords: Gold; Clusters; Nanoparticles; AFM; Conductivity; Lithography

1. Introduction

Metal nanoparticles are receiving a great deal of attention because of their wide range of applications [1] in areas, such as catalysis [2], chemical sensing [3–12], nanoelectronics [13], separations [1,14], surface-enhanced Raman scattering [15], and biological imaging [1]. There is particular interest in their optical and electronic properties which have been recently exploited for optical [3,4], electrochemical [5], and electronic-based [6–12] chemical sensing and for designing single electron transistors [16–18]. Further fundamental studies are needed to gain a better understanding of how these properties are affected and controlled by particle size and chemical environment.

* Corresponding author.
E-mail address: f.zamborini@louisville.edu (F.P. Zamborini).
[1] Present address: Chemistry Department, Gottwald Science Center, University of Richmond, Richmond, VA 23173, USA.

0003-2670/$ – see front matter © 2003 Elsevier B.V. All rights reserved.
doi:10.1016/j.aca.2002.10.003

For most applications it is equally important to design strategies for assembling and patterning well-ordered one-dimensional [19], two-dimensional [20], and three-dimensional arrays of metal nanoparticles.

In this paper we determine the concentration and average core edge-to-edge spacing (δ_e) in network films of Au_{140} monolayer-protected clusters (MPCs) and correlate it to previously reported [11] electronic conductivity measurements on identically-prepared films [21–23]. This was accomplished by measuring the physical thickness and the optical absorbance of the films with atomic force microscopy (AFM) and UV-Vis spectroscopy, respectively. The films are comprised of Au_{140} clusters surrounded by a mixed monolayer of *n*-alkanethiolates ("non-linker") and mercaptoundecanoic acid (MUA, "linker") and were assembled by linking the nanoparticles with previously described [11,24–28] carboxylate–Cu^{2+}–carboxylate coordination. The chainlength of the "non-linker" *n*-alkanethiolates was varied between 4, 8, and 12 carbons while the "linker" was kept constant (these clusters are referred to as C4/MUA, C8/MUA, and C12/MUA Au MPCs). We found that δ_e increases with increasing chainlength (C4 < C8 < C12) and a plot of $\ln(\sigma_{EL})$ versus average δ_e gives an electronic coupling factor (β) of $1.2\,Å^{-1}$, which is consistent with previous reports on tunneling through hydrocarbons [29–37]. Measured electron transfer rate constants of the films reflect the increased cluster spacing with increasing non-linker chainlength. We also patterned films by AFM- and scanning tunneling microscope (STM)-based lithography with sub-100 nm resolution.

The gold nanoparticles in this study are referred to as monolayer protected clusters (MPCs) [21–23] to emphasize the stabilizing aspect of the thiolate ligand shells. Their electronic communication has been investigated via the electronic conductivities of cast, non-networked films of arylthiolate [38] and of alkanethiolate-coated [35,36] MPCs. Within these studies, it has been shown that electronic communication between the metal-like MPC cores occurs by electron hopping (self-exchange), with the intervening monolayer coatings serving as tunneling bridges. Results showed that electronic conductivity is a bimolecular process with an extremely fast rate constant that varies exponentially with the core edge-to-edge spacing as expected for an electron tunneling reaction [35]. Cast films of MPCs with reasonably uniform Au core sizes and observable solution quantized double layer charging [24,39] properties could be prepared with well-defined mixtures of different core electronic "charge states" [35]. The large rate constants and small activation barriers are consistent with Marcus relationships [40–42], and in summary, arise from the low dielectric medium surrounding the Au core reaction centers and the relatively large size of those centers.

We previously investigated the electronic communication between MPC cores in monolayer [27] and multilayer [28] films of Au_{140} nanoparticles containing mixed monolayers of hexanethiolate and MUA that were linked by metal ion-carboxylate coordinative coupling. Electrochemical investigations of films in contact with CH_2Cl_2/electrolyte solutions showed heterogeneous electron transfer rate constants of $10^2\,s^{-1}$ for a monolayer [27] of nanoparticles and nanoparticle–nanoparticle self-exchange electron transfer rate constants of $10^6\,s^{-1}$ for multilayer films [28]. It was surmised that electron tunneling proceeds through different pathways; the metal-linked MUA ligands in monolayer films and the non-bonded hexanethiolates in multilayer films.

In a later report [11], air-dried films of mixed monolayer Au MPCs linked by carboxylate–Cu^{2+}–carboxylate bridges showed that the electronic conductivity (σ_{EL}) proceeds primarily through the non-linker, non-bonded contacts and changes by 3 orders of magnitude depending on the chainlength. A linear plot of $\ln(\sigma_{EL})$ versus chainlength showed that conductivity occurs by electron hopping (tunneling) between the Au_{140} cores via the non-linker chains, but limited information on the packing arrangement of the film and average edge-to-edge cluster spacing prevented accurate determinations of the electronic coupling factor (β) and electron transfer rate constants. Conductivity was sensitive to the bathing medium (air, N_2, liquids) and the films demonstrated chemiresistive, microgravimetric, and spectroscopic responses toward ethanol vapor, implying possible applications in chemical sensing.

Others have assembled films of Au nanoparticles through hydrogen bonding [8], dithiols [43–46], DNA [47], covalent binding [48], electrostatic attraction [49], polyelectrolytes [50–52], and dendrimers [9,12] and studied their electronic properties or potential use as chemiresistive sensors. There are also

several approaches for assembling nanoparticles in the solution-phase through biological recognition [53], DNA [54–56], metal ions [4,26], dithiols [57,58], C60 [59], or cyclodextrins [60]. Patterning films of MPCs or Au colloids is essential for fabricating miniaturized devices based on these materials. Microcontact printing [61,62], electron-beam lithography [63,64], AFM [65–70], and STM [71,72] lithography are recent examples. A series of papers showed that the manipulation and assembly of individual nanoparticles with scanning probe tips is possible [66–70]. Development of novel strategies for patterning Au nanoparticles will make it possible to study their properties on the nano-scale and reduce the size of nanoparticle-based electronic and chemical sensing devices.

2. Experimental

2.1. Chemicals

All chemicals were reagent grade and used as received.

2.2. Synthesis and preparation of mixed monolayer MPCs

Alkanethiolate monolayer-protected clusters (MPCs) were synthesized using a modified Brust reaction [22]. Briefly, butanethiol (C4), hexanethiol (C6), octanethiol (C8), or dodecanethiol (C12) were combined in toluene in a 3:1 mole ratio with $AuCl_4^-$, followed by a 10-fold excess of reductant ($NaBH_4$ in water) at 0 °C. The MPC product was recovered from the stirred reaction mixture after 24 h by precipitation, filtering, and thorough washing with acetonitrile on a glass fritted Buchner funnel. We label this 28 kDa product as C*n* MPC, where *n* is the number of carbons in the alkanethiolate chain.

Linker ligand 11-mercaptoundecanoic acid (HS$(CH_2)_{10}CO_2H$, MUA) was place-exchanged [73] for some of the *non-linker* C*n* ligands in the initial MPC monolayer. Stirring tetrahydrofuran (THF) solutions of MPC and linker ligand (in selected molar ratios) for ca. 4 days gave mixed monolayer MPCs that were collected and washed as above. The mole ratio of linker to non-linker thiolates was determined by NMR of solutions of the disulfides that were quantitatively liberated from the mixed monolayer MPCs upon decomposition with iodine [73].

Based on transmission electron microscopy (TEM) and thermogravimetry as described previously [74], the C*n* MPCs have *average* core diameters of 1.6 ± 0.8 nm and $Au_{140}(Cn)_{53}$ composition. The MPCs with mixed monolayers containing MUA have (by NMR) the *average* composition $Au_{140}(Cn)_{33}(MUA)_{20}$. The compositions are averages in that a dispersion of Au core sizes exists (as determined by TEM). Additionally, some dispersity in the C*n*/MUA ligand ratio is statistically expected within the overall MPC population.

2.3. Patterning MPC films on gold by microcontact printing

Films of C*n*/MUA mixed-monolayer protected clusters were microcontact printed on Au films as shown in Scheme 1. First, an Au film was

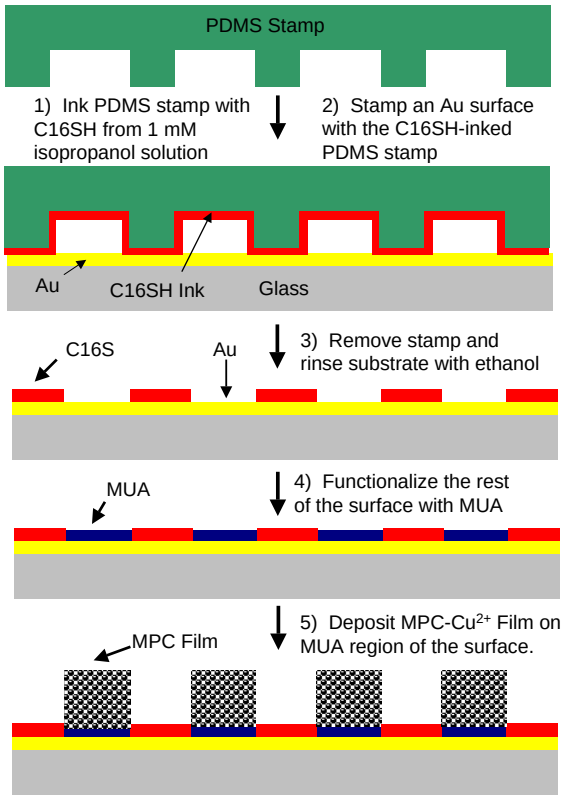

Scheme 1.

cleaned by rinsing with ethanol, rinsing with isopropanol, drying under nitrogen, and placing in a UV ozone cleaner for 10 min (Jelight Company Inc., Irvine, CA). A polydimethylsiloxane (PDMS) polymer stamp (gift from Professor Mark Schoenfisch, UNC-Chapel Hill) was inked in a 2 mM hexadecanethiol (C16SH)/isopropanol solution and dried under nitrogen. Then, using a procedure developed by Whitesides [75], the PDMS stamp was brought into contact with the clean Au surface for 1–2 min to create a pattern of the C16S self-assembled monolayer (SAM). The Au surface was rinsed thoroughly with ethanol and dried under nitrogen. The Au was then placed in a 2 mM ethanol solution of MUA for 15 min to fill in the unpatterned regions with the ω-carboxylic acid-functionalized SAM. Au C*n*/MUA MPCs were deposited on the MUA regions using a previously described procedure [11,24,27,28]. Briefly, the sample was soaked in a 0.1 M $Cu(ClO_4)_2$/ethanol solution for 10 min, rinsed with ethanol, and placed in an approximately 1–2 mg/ml ethanolic solution of the appropriate C*n*/MUA MPCs for 20–30 min. This constitutes one "dip cycle" and by repeating the procedure thick films were prepared. The procedure above results in a patterned Au surface containing regions of Au/C16S and regions of Au/MPC Film (Fig. 1). It is important to note that when several dip cycles were used a visible amount of MPCs accumulated on the Au/C16S region as well. In this case, Scotch tape was used to remove these physisorbed MPCs, which were easily dislodged without perturbing the MPC film that had been grown on the Au/MUA regions.

2.4. Preparing MPC films on glass

MPC films were deposited on a glass slide using previously described [11,24,25] carboxylate–Cu^{2+}–carboxylate chemistry as follows: a layer of 3-mercaptopropyltrimethoxy silane (MPTMS) [76] was attached to the glass surface by exposing it to 100 μl of MPTMS in 10 ml isopropanol (plus two to three drops deionized water) and heating to near boiling for 30 min. The slide was rinsed with ethanol, dried under a N_2 stream, and heated at 100 °C for 5–10 min. The slide was then serially exposed to 0.1 M $Cu(ClO_4)_2 \cdot 6H_2O$ in ethanol (10 min), rinsed with ethanol, exposed to 1–2 mg/ml MPC in ethanol (20–30 min), rinsed with ethanol, and then dried under N_2. This protocol, a "dip cycle," deposits several monolayers of MPCs. Additional dip cycles serve to build up the network film thickness.

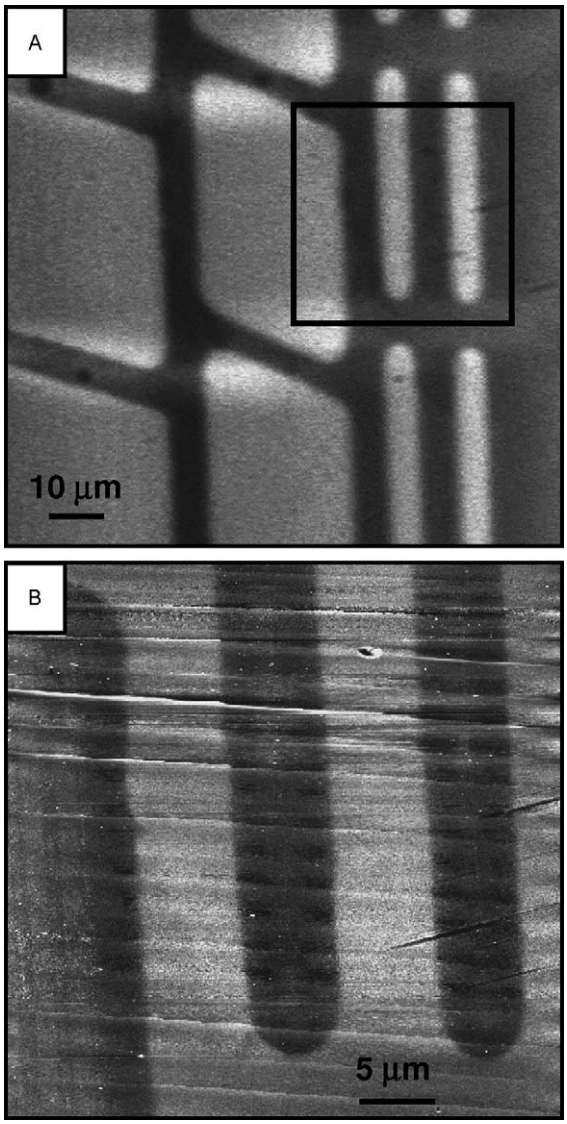

Fig. 1. (A) Optical and (B) AFM image of a C6/MUA MPC film microcontact printed on an Au substrate. The film was deposited using two dip cycles and the procedure outlined in Scheme 1. The square in Frame A corresponds to the approximate area imaged with AFM in Frame B. Opposite contrast is observed for the two images due to the different imaging mechanisms. Au/C16S regions appear bright in the optical image, but dark in the AFM image, and vice versa for the Au/MPC regions.

2.5. Absorbance and thickness measurements

Absorbance spectra were obtained from 300 to 1000 nm on MPC-coated glass slides using a Varian Cary 50 UV-Vis spectrophotometer and subtracted from a spectrum of bare glass. The quantity of MPCs deposited was determined spectrophotometrically at 520 nm based on $\varepsilon_{Au140} \approx 3.8 \times 10^5\,M^{-1}\,cm^{-1}$ [77]. Film thicknesses were measured on MPC films patterned on Au with a Veeco Metrology Digital Instruments (Santa Barbara, CA) Nanoscope IIIA multimode AFM. Silicon tips were scanned over the edge of the film in tapping-mode and the thickness was determined by performing an average cross-sectional analysis (Fig. 2). The thickness was measured in at least two different regions on each sample. The glass and patterned Au samples were treated with identical Cu^{2+} and MPC solutions using the same soaking times as described above in order to ensure that the films were deposited similarly on both substrates and that the absorbance measured on glass could be correlated with the thickness measured on the patterned Au. Between four and six dip cycles were typically used to deposit the films.

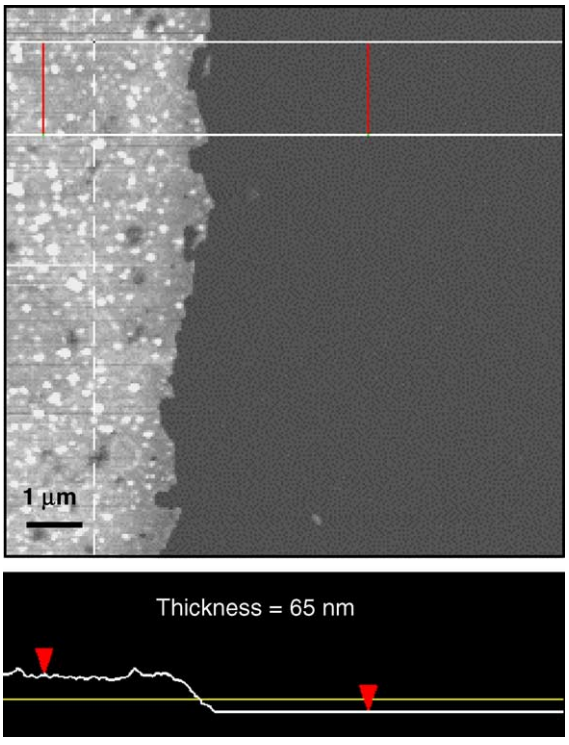

Fig. 2. An AFM image (top) showing the edge of a patterned C8/MUA MPC film on an Au substrate and the corresponding cross-sectional line scan (bottom) used to obtain the film thickness. This film was 65 nm thick.

2.6. Electronic conductivity

Solid-state electronic conductivity measurements from a previous report were employed [11].

2.7. Scanning probe lithography

A Veeco Metrology Digital Instruments (Santa Barbara, CA) Nanoscope IIIA multimode atomic force microscope (AFM) and STM were used to perform scanning probe lithography experiments on various MPC films. Films on Au and glass were patterned by scanning a particular region of the film with a silicon nitride AFM tip in contact mode with a 20 V deflection setpoint (1.0×10^{-6} to 1.7×10^{-8} N) and scan rate of 5 Hz for 1–10 min as indicated. A cut Pt/Ir STM tip (Veeco Metrology Digital Instruments, Santa Barbara, CA) was used to pattern films deposited on Au by scanning the desired region under normal imaging conditions (0.5 V bias, 1 nA tunneling current, 3–5 Hz scan rate) for 10–15 min typically. Patterns were formed by selective removal of the film under the scanned area. Films patterned on glass with AFM were subsequently heated to 300 °C for 10 min in a vacuum tube furnace (Lindbarg Blum) to fabricate patterned films of metallic Au on glass [25].

3. Results and discussion

3.1. Determination of edge-to-edge cluster spacing (δ_e)

Measuring the concentration and average core edge-to-edge spacing in films of clusters is crucial when studying their electronic properties because conductivity proceeds by electrons hopping (or tunneling) from core-to-core, which is largely dependent on the distance between the particles and the chemical composition of the tunneling barriers. Electron hopping kinetics can also be analyzed when

the average spacing is known. The measurements are analytically challenging because direct images of individual, adjacent nanoparticles are not easily obtained in these three-dimensional films. There are other methods available, however, for obtaining core edge-to-edge distances. For example, small angle X-ray scattering (SAXS) [55] was used to measured interparticle distances of DNA-linked Au nanoparticles and pycnometry [35,38] was used to measure the concentration of drop-cast MPC films. Both studies correlated the information with the electrical properties. It is also possible to determine the concentration of MPCs in films by measuring both MPC coverage and film thickness. Coverage has been previously measured spectroscopically [25] and electrochemically [24,27,28] while thickness has been measured by profilometry [25] and AFM [62].

In this paper the goal was to determine and compare the average cluster spacing in films of C4/MUA, C8/MUA, and C12/MUA MPCs[2] and correlate the data with previously measured electronic conductivity measurements on identical films. This has been accomplished by devising experiments suited to measuring the physical thickness and optical absorbance of films that were identically prepared on Au and glass samples, respectively. Thickness was measured with AFM on Au substrates patterned with C*n*/MUA MPC films by microcontact printing (see Scheme 1) [75]. A PDMS stamp was inked with C16SH and brought into contact with a clean Au substrate. The Au substrate was rinsed with ethanol and exposed to an ethanolic solution of MUA for 15 min. This produces an Au substrate patterned with C16S and MUA. We then selectively deposited the C*n*/MUA MPC film onto the MUA region of the sample using previously described [11,24,27,28] carboxylate–Cu^{2+}–carboxylate chemistry, creating a Au substrate patterned with the MPC film. Others have similarly prepared well-defined micron-sized patterns of Au clusters by microcontact printing [61,62].

Fig. 1 shows an optical micrograph and AFM image (Frames A and B, respectively) of an Au C6/MUA MPC film patterned onto an Au substrate (two dip cycles) using the procedure in Scheme 1. In the optical image (Frame A), the bright regions correspond to Au/C16S and the dark regions to Au/MPC film because the MPC film is black. In AFM (Frame B), the bright regions correspond to Au/MPC film and the dark regions to Au/C16S because the AFM maps out topography, designating taller regions brighter. The box in Frame A is the approximate region scanned by the AFM as shown in Frame B. The patterns are very sharp and well-defined, which is consistent with previous examples of microcontact printed SAMs [75]. The MPC film clearly grows selectively on the MUA region and does not grow laterally to a noticeable extent when only two dip cycles are used. Importantly, we were able to scan over the patterns and obtain an accurate measurement of the thickness of these films using AFM.

Fig. 2 shows the AFM image of an edge on a patterned C8/MUA MPC film on Au and the cross-sectional analysis that was employed for determination of the film thickness. The bright region corresponds to the C8/MUA MPC film and the dark region corresponds to Au/C16S. In this case the thickness of the film was approximately 65 nm. Fig. 3 shows the UV-Vis spectrum of the C8/MUA film on glass that was prepared in parallel to the film shown in Fig. 2. It is characterized by an exponential decrease in absorbance over the scanned wavelengths with a small, broad peak near 550 nm, consistent with small

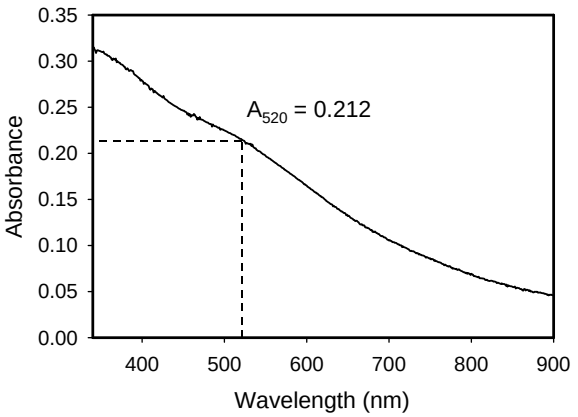

Fig. 3. UV-Vis absorbance spectrum of a C8/MUA MPC film deposited on glass after subtraction of a bare glass spectrum. The absorbance decreases with increasing wavelength and there is a small, broad peak near 550 nm, consistent with the assembly of tiny, aggregated clusters in the film. Absorbance was measured at 520 nm for the MPC concentration and edge-to-edge spacing analysis.

[2] A single sample of C6/MUA was also tested, but the results were not included in this paper.

Table 1
Data used to calculate concentration and average spacing of MPC films

MPC film	Thickness, l (nm)	Absorbance, $A/2$	C_{MPC} (MPCs/cm^3)	Edge-to-edge spacing, δ_e (Å)
C4/MUA	100	0.245	3.88×10^{19}	13.5
	55	0.125	3.60×10^{19}	14.3
	90	0.149	2.62×10^{19}	17.7
				Average $\delta_e = 15.2 \pm 2.2$
C8/MUA	65	0.148	3.61×10^{19}	14.3
	170	0.187	1.74×10^{19}	22.6
	65	0.106	2.58×10^{19}	17.8
	80	0.109	2.16×10^{19}	19.9
	115	0.231	3.18×10^{19}	15.6
				Average $\delta_e = 18.0 \pm 3.3$
C12/MUA	70	0.120	2.72×10^{18}	17.3
	50	0.040	1.27×10^{19}	26.9
	35	0.054	2.44×10^{19}	18.5
	90	0.119	2.09×10^{19}	20.3
	80	0.128	2.53×10^{19}	18.0
				Average $\delta_e = 20.2 \pm 3.9$

clusters that have been aggregated by binding between their monolayers [11]. The absorbance was measured at 520 nm for the analysis of MPC concentration and core edge-to-edge spacing. The thicknesses and corresponding 520 nm absorbances measured for three or more samples of C4/MUA, C8/MUA, and C12/MUA MPC films are displayed in Table 1.

The average core edge-to-edge cluster distance (δ_e), calculated from the thickness and absorbance data, for each film is also displayed in Table 1. The spacing was calculated as follows: the 520 nm absorbance of each film was converted to MPC coverage using

$$\frac{A}{2} = \varepsilon \Gamma_T \times 1000 \quad (1)$$

where A is absorbance at 520 nm, ε the molar absorptivity ($3.8 \times 10^5\ M^{-1}\ cm^{-1}$) [77] and Γ_T the coverage of MPCs in mol/cm^2. A is divided by 2 to account for the film growing on both sides of the glass. The concentration of MPCs in the film was calculated based on the cubic lattice model shown in Scheme 2, using

$$C_{MPC} = \frac{N\Gamma_T}{l} \quad (2)$$

where N is Avogadro's number, l the thickness of the film, and C_{MPC} the concentration in MPCs/cm^3. The resultant MPC core edge-to-edge distance (δ_e, cm) separating two adjacent clusters is

$$\delta_e = z - d = \left(\frac{1}{C_{MPC}}\right)^{1/3} - 1.6 \times 10^{-7} \quad (3)$$

where the right-hand term corrects for the average diameter (d) of the MPCs used in this study.

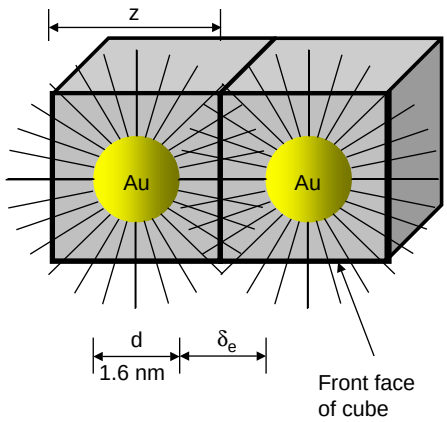

$\delta_e = z - d$

$= (1/C_{MPC})^{1/3} - 1.6 \times 10^{-7}$ cm

Scheme 2.

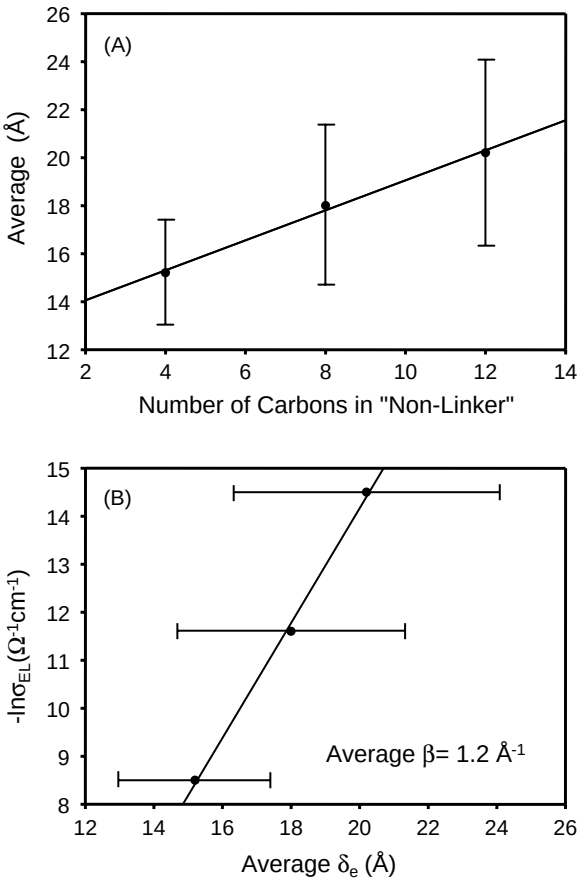

Fig. 4. (A) Plot of average edge-to-edge distance (δ_e) vs. the number of carbons in the non-linker chainlength and (B) $-\ln(\sigma_{EL})$ vs. δ_e for the various MPC films studied (C4/MUA, C8/MUA, and C12/MUA). The data are displayed in Tables 1 and 2. δ_e increases linearly with increasing chainlength and σ_{EL} increases exponentially with decreasing chainlength (or decreasing δ_e) as expected for a electron tunneling process.

Fig. 4A shows a plot of the calculated average δ_e versus the number of carbons (C*n*) in the non-linker ligand. The average δ_e in films of C4/MUA, C8/MUA, and C12/MUA MPCs is 15.2 ± 2.2, 18.0 ± 3.3, and 20.2 ± 3.9 Å, respectively. For comparison, the approximate lengths of C4, C8, C12, and MUA molecules are 9, 14, 19, and 19 Å, respectively, assuming the ligands are fully extended with respect to the surface normal and in an all-trans conformation [78,79]. Clearly the cluster spacing is not determined by head-to-head linking of the MUA ligands (Au–S$(CH_2)_{10}CO_2Cu^{2+}O_2C(CH_2)_{10}$S–Au), since this would give similar spacings of 38 Å (2MUA) for each of the cluster films. As we concluded previously [11], the spacing is determined by the length of the non-bonded, non-linker C*n* alkanethiolates. The expected spacing for head-to-head packing of the non-linker (Au–SC*n*-C*n*S–Au) would be 18, 28, and 38 Å, for C4, C8, and C12, respectively (2C*n*). Since these values are all larger than the measured values, we conclude that the non-linker ligands are interdigitated to some degree in each of the cluster films studied. The degree of interdigitation was calculated as a percentage using

$$\text{Interdigitation (\%)} = \frac{2t_{Cn} - \delta_e}{t_{Cn}} \times 100 \quad (4)$$

where t_{Cn} is the theoretical length of the non-linker ligand as indicated above (C4 = 9 Å) and δ_e the measured core edge-to-edge spacing. The calculated percentage interdigitation is 31, 71, and 94% for C4, C8, and C12 ligands in the cluster films, respectively. Chain interdigitation is theoretically predicted and has been observed experimentally from TEM and density measurements for drop-cast, non-linked films of Au MPCs [35]. The observed cluster spacing in TEM is approximately the length of one chainlength (full interdigitation) and the extent of interdigitation is not chainlength dependent as observed in this study. The MUA–Cu^{2+}–MUA linkage in our MPC films clearly inhibits interdigitation for short chainlengths more than the longer C12 ligands. The *number* of MUA ligands per MPC was kept constant between samples in this study because it is also likely to affect chain interdigitation. It is surprising that interdigitation is not inhibited more by the long MUA–Cu^{2+}–MUA linkage. MUA chain flexibility and hydrophobic interactions between the alkanethiolates likely account for the extent of interdigitation. The hydrophilic Cu^{2+}–carboxylates and carboxylic acid groups of MUA may also avoid the hydrophobic alkane chains and cause some microheterogeneity, allowing the clusters to pack efficiently.

The large error bars in the Fig. 4 plots reflect the amount of uncertainty in the calculated δ_e. Correlating the AFM thickness with optical absorbance gives only an estimate of δ_e and there are possible sources of error, leading to this uncertainty. First, the average diameter of the clusters in the films may not be

exactly 1.6 nm even though that is the average diameter of clusters in the MPC solutions used to prepare the films. Second, absorbance and thickness are measured from two different kinds of samples (glass and Au). Differences in film growth on the two samples could lead to some error, however, comparison of the absorbance of MPC films deposited on transparent Au and glass samples indicate that the growth is similar on both samples. Finally, non-uniformity in the films could lead to small errors in the measured AFM thicknesses. Each of these sources of error could vary from experiment to experiment. The experiments were repeated several times and averaged (Table 1) in order to minimize these uncertainties.

3.2. Correlating edge-to-edge distance (δ_e) with electronic conductivity

A previous report [11] showed that the electronic conductivity of identically prepared films varied by three orders of magnitude and was exponentially dependent on the non-linker chainlength. A linear plot of $\ln(\sigma_{EL})$ versus chainlength indicated an electron tunneling, or hopping mechanism, between the non-bonded alkanethiolates, but the actual cluster–cluster distances were not measured. Electronic conductivity in terms of δ_e and temperature (T) is given by [38]

$$\sigma_{EL}(\delta_e, T) = \sigma_0 \exp[-\beta_d \delta_e] \exp\left[\frac{-E_A}{RT}\right] \quad (5)$$

where σ_{EL} is electronic conductivity ($\Omega^{-1}\,cm^{-1}$), δ_e the core edge-to-edge distance (cm), β_d is electron-tunneling coefficient ($Å^{-1}$), E_A is activation barrier energy (kJ/mol), R the gas constant, and T the temperature in K. A plot of $\ln(\sigma_{EL})$ versus δ_e is shown in Fig. 4B. The slope of the plot, a measurement of β_d, is 1.2 $Å^{-1}$. This is in close agreement with values measured for electron tunneling through saturated hydrocarbons in solid-state conductivity measurements of drop-cast Au clusters [35,36] (0.8–1.2 $Å^{-1}$), electrochemical measurements of ferrocene (Fc)-terminated self-assembled monolayers (SAMs) (0.85–1.0 $Å^{-1}$) [29–31], AFM-based conductivity measurements through alkanethiol SAMs [34] (1.1 $Å^{-1}$), and conductivity through SAMs on closely spaced Hg (0.89 C^{-1}) [37] or Ag and Hg surfaces (0.87 $Å^{-1}$) [32,33].

Table 2
Conductivity and kinetic data for various MPC films

MPC film	Average δ_e (Å)	σ_{EL} ($\Omega^{-1}\,cm^{-1}$)	k_{ET} (s^{-1})
C4/MUA	15.2 ± 2.2	2×10^{-4}	5×10^{7}
C8/MUA	18.0 ± 3.3	9×10^{-6}	3×10^{6}
C12/MUA	20.2 ± 3.9	5×10^{-7}	2×10^{5}

The first-order electron transfer rate constant for the bimolecular self-exchange process between adjacent MPCs is given by [38]

$$k_{ET}\,(s^{-1}) = \frac{6RT\sigma_{EL}}{F^2\delta_c^2} \quad (6)$$

where R is the gas constant, T the temperature in K, σ_{EL} the electronic conductivity ($\Omega^{-1}\,cm^{-1}$), F the Faraday constant, δ_c the average core center-to-center separation (δ_e + 16 Å), and C the concentration of MPCs in the film (mol/cm^3). This equation assumes that electronic charge is localized on MPC cores as electron donor–acceptor reactants and that the charge carrier concentration equals the MPC core concentration [35,38]. The results are displayed in Table 2. They reflect the chainlength dependence and are similar to previous kinetic analyses of drop-cast MPC assemblies. The rate constant for the C4/MUA film, where electrons are tunneling ca. 15 Å, is $5\times10^7\ s^{-1}$. This is the same order of magnitude compared to solid-state, drop-cast films of Au cluster–alkanethiol–Au cluster tunnel junctions (Au C10 MPCs, $\delta_e \sim 15$ Å) [35], and several orders of magnitude faster than electron transfer rate constants measured electrochemically through redox polymers [80] and Au–alkanethiol–Fc [29–31] tunnel junctions. The large rate constants are consistent with Marcus relationships [40–42], arising from the low dielectric medium surrounding the Au core reaction centers and the large size of those centers.

3.3. AFM and STM patterning of Au MPC films

Another goal of this paper is to show that films of MPCs can be patterned with scanning probe lithography in a straight-forward manner with nanometer resolution. Patterning films of metal nanoparticles on the nano-scale is essential if they are going to find use as the components of nano-chemical sensors or electronic devices for future technological applications.

AFM- and STM-based lithography experiments that utilize physical force, electrochemistry, or other mechanisms are well-known on SAM- [81–83], polymer- [84,85], dendrimer [86], oxide- [87] and nanoparticle-modified [65–72] surfaces. These techniques are capable of producing well-defined patterns at the nanometer-scale. In this paper we used AFM and STM to pattern MPC films with nanometer

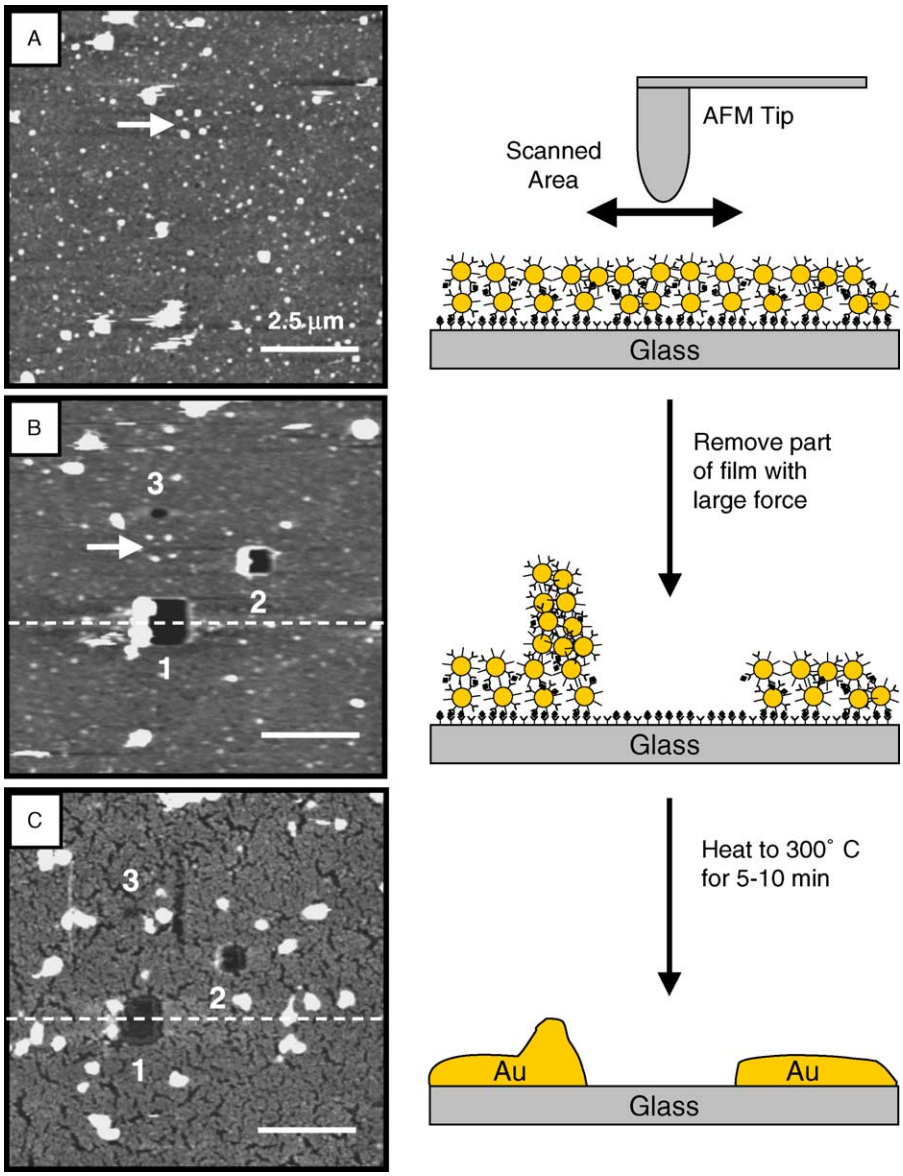

Fig. 5. Contact-mode AFM images demonstrating the selective removal of MPC films with the scanning probe tip. (A) 10 μm × 10 μm image obtained on a glass surface modified with a C12/MUA MPC film before patterning using a deflection setpoint of 2.0 V. (B) Same 10 μm × 10 μm area obtained using a deflection setpoint of 2.0 V after patterns of 1 μm × 1 μm, 500 nm × 500 nm, and 100 nm × 100 nm (points 1, 2, and 3, respectively) were prepared by scanning those regions with a deflection setpoint of 20.0 V. (C) Same 10 μm × 10 μm image obtained after heating the sample to 300 °C for 10 min in a vacuum tube furnace. The arrow in Frames A and B show the same area (four bright dots) to aid comparing of the images before and after patterning.

resolution by physically removing clusters in the scanned region with the scanning probe tip.

Fig. 5 shows the results of an AFM lithography experiment on a glass surface modified with a C12/MUA film and the corresponding illustration. At low deflection setpoints (2.0 V), the MPC film was imaged with a silicon nitride tip in contact mode for long periods of time without degradation or instability of the surface (Frame A). At a deflection setpoint of 20 V, the tip removes the film in the scanned region through a physical scratching mechanism. Frame B shows 1 μm × 1 μm, 500 nm × 500 nm, and 100 nm × 100 nm patterns (labeled as points 1, 2, and 3, respectively) that were fabricated by scanning those areas with a 20 V setpoint for 10, 5, and 1 min, respectively. The dark squares correspond to areas where the clusters were removed and the bright regions at the edges are where the displaced clusters accumulated. Fairly large forces were required to remove the cluster film (1.0×10^{-6} to 1.8×10^{-8} N), showing that the MPC network film is held together very strongly through the carboxylate–Cu^{2+}–carboxylate bridges. Patterns 1 and 2 (labeled on figure) were well-defined, but pattern 3 was relatively blurred due to the pattern size approaching the tip radius of curvature. The overall quality of the image in Frame B is much lower compared to Frame A, implying that the AFM tip suffers some damage during the patterning process. The arrow in Frames A and B indicates the same region on the surface to aid comparing of the images before and after patterning.

We previously reported on the preparation of metallic films from MPC precursors by assembling MPC films on glass as described in this paper and then subsequently heating them to 300 °C for 5–10 min [25]. This process removes the organic monolayer surrounding the clusters and allows them to coalesce into a smooth metallic Au film. The films were smooth, adherent, and conductive, but also contained impurities of Cu and S. Nevertheless, we demonstrated a simple benchtop method for preparing metal films without the need for high vacuum equipment and with the added benefit that metal could be deposited on irregular or highly-confined surfaces.

Fig. 5C shows the patterned C12/MUA Au MPC film from Fig. 5B after heating to 300 °C for 5–10 min as discussed earlier. Three observations were made. (1) The appearance of the film changed dramatically from a continuous rough film (RMS = 16.5 nm) to a smoother, grainier film following heat treatment (RMS = 13.7 nm). (2) Patterns 1 and 2 retain their shape quite well, but pattern 3 was no longer noticeable after heating. This limits the resolution of this method to ca. 100 nm. (3) Cross-sectional analysis (dashed lines) of the 1 μm × 1 μm pattern before and after heating reveal that the film has decreased in thickness from 50 to 20 nm, or ∼60% (see Fig. 6). This is consistent with the analysis of the average δ_e calculated for a C12/MUA MPC film. The thickness per layer of the C12/MUA film before heating is equal to the average d of the clusters (16 Å) plus the average δ_e (20 Å), or 36 Å. The thickness per layer after heating is equal to *d*, or 16 Å. A thickness change from 36 to 16 Å corresponds to 56%, which is very close to the measured 60% change.

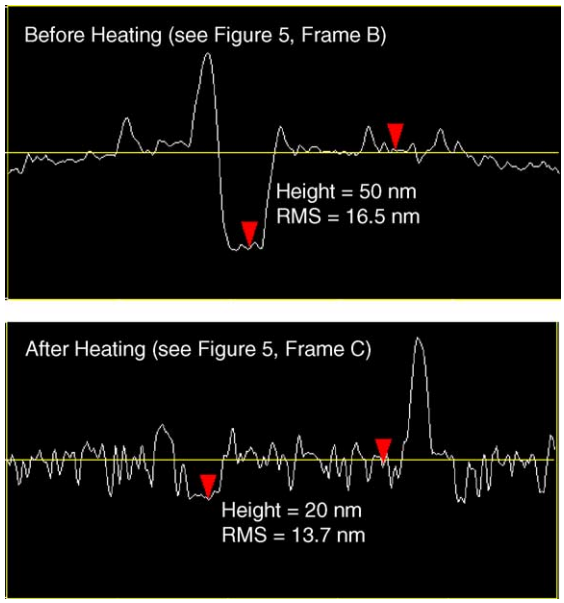

Fig. 6. Cross-sectional line scans of the 1 μm × 1 μm pattern from Fig. 5 (Frames B and C) before and after heating (top and bottom frames, respectively). The film becomes smoother and the thickness decreases from 50 to 20 nm (60%) upon heating.

Importantly, our method produces patterns of Au on glass using simple benchtop chemistry, AFM lithography, and heating, where the MPCs act as precursors to the metal film. This may be a useful and cost-efficient approach for preparing closely-spaced metal contacts to study the electronic properties of carbon nanotubes, silicon nanowires, or other interesting nanomaterials.

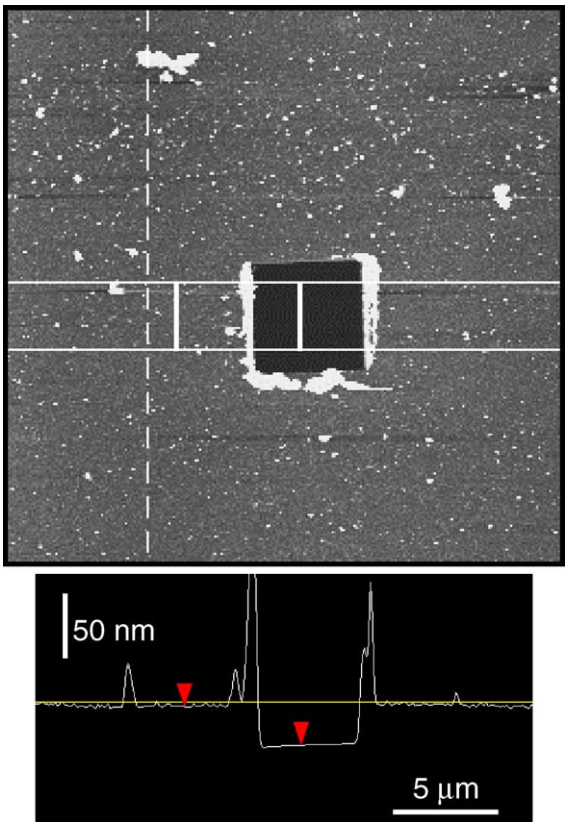

Fig. 7. A tapping-mode AFM image showing a 5 μm × 5 μm square pattern that was fabricated on a C12/MUA MPC film on an Au substrate with a Pt/Ir STM tip. The pattern was prepared by scanning the area for 15 min at a bias of 0.5 V and tunneling current of 1.0 nA. The cross-sectional line scan shows that the thickness of the film was approximately 31 nm.

It is also possible to pattern the Au MPC films with STM. Fig. 7 shows a tapping-mode AFM image of a 5 μm × 5 μm square pattern that was fabricated on a C12/MUA MPC film on Au with STM at a bias of 0.5 V and tunneling current of 1.0 nA for ca. 15 min. The dark square again corresponds to the region where clusters were removed and bare Au or Au/MUA is presumably exposed. The bright regions correspond to clusters that were removed from the scanned area and subsequently accumulated on the edges of the pattern. The removed clusters accumulated more evenly around the pattern compared to the AFM experiments (Fig. 5B), where removed clusters were predominantly located on one side of the pattern. Patterning occurs with STM because the conductivity of the MPC film is not sufficient to support electron tunneling from the tip through the film. Instead, the tip physically moves through the film and removes MPCs in the scanned area as electrons tunnel from the tip to the underlying Au substrate. Recently, Meldrum and co-workers reported a bias-dependent manipulation of individual dodecanethiol-coated Au nanoparticles on a graphite surface with an STM tip [71]. At low bias, the electrons at the STM tip do not have sufficient energy to overcome the Coulomb blockade and the tip pushes into and moves the Au nanoparticle. At high bias, the energy is sufficient for the electrons to tunnel from the tip to the cluster and the tip images above the nanoparticle without altering it. We did not observe a bias dependence in our studies, but more work needs to be done. STM is not capable of patterning films prepared on glass or other non-conductive samples, which limits possible lithography applications.

4. Conclusions

We have demonstrated a method for determining the average cluster edge-to-edge distance in films of mixed-monolayer C*n*/MUA MPCs using a combination of AFM and UV-Vis spectroscopy (the methodology employed should be amenable to other electronically conductive films). The average cluster spacing increased linearly with the non-linker (C*n*) chainlength in the order C12 > C8 > C4. A plot of $\ln(\sigma_{EL})$ versus the average cluster spacing was also linear and the slope gave a β value equal to 1.2 $Å^{-1}$, consistent with electron tunneling through saturated hydrocarbons. Kinetic studies revealed fast electron-transfer kinetics between adjacent clusters, consistent with previous experiments on MPC assemblies. Nanoscale patterning of the films was demonstrated using AFM and STM and subsequent heating of patterned films on glass led to patterned metallic Au films. Changing the ligand composition and chainlength of assembled MPCs allows control over their electronic properties and a better fundamental understanding of these effects continues to be an important objective. Further, future applications of metal nanoparticles will require them to be controllably assembled and patterned on the nano-scale.

Studies of other factors affecting the electronic conductivity and average cluster spacing, such as the

effect of different ligand compositions (aromatic and rigid groups) and metal cation linkers, are currently underway. We hope to better understand what controls the assembly and packing of three-dimensional MPC films formed by our approach and to understand the effect of chemical environment and structure on electron hopping conductivity.

Acknowledgements

This research was supported in part by research grants from the National Science Foundation and the Office of Naval Research. F.P.Z. acknowledges financial support from the University of Louisville. L.E.S. acknowledges financial support from the University of Louisville Summer Research Opportunity Program (SROP).

References

[1] C.R. Martin, D.T. Mitchell, Anal. Chem. 70 (1998) 322A–327A.
[2] R.M. Crooks, M. Zhao, L. Sun, V. Chechik, L.K. Yeung, Acc. Chem. Res. 34 (2001) 181–190.
[3] R. Elghanian, J.J. Storhoff, R.C. Mucic, R.L. Letsinger, C.A. Mirkin, Science 277 (1997) 1078–1080.
[4] Y. Kim, C.S. Johnson, J.T. Hupp, Nano Lett. 1 (2001) 165–167.
[5] A.N. Shipway, E. Katz, I. Willner, Chem. Phys. Chem. 1 (2000) 18–52.
[6] H. Wohltjen, A.W. Snow, Anal. Chem. 70 (1998) 2856–2859.
[7] S.D. Evans, S.R. Johnson, Y.L. Cheng, T. Shen, J. Mater. Chem. 10 (2000) 183–188.
[8] L. Han, D.R. Daniel, M.M. Maye, C.-J. Zhong, Anal. Chem. 73 (2001) 4441–4449.
[9] N. Krasteva, I. Besnard, B. Guse, R.E. Bauer, K. Mullen, A. Yasuda, T. Vossmeyer, Nano Lett. 2 (2002) 551–555.
[10] S.-J. Park, T.A. Taton, C.A. Mirkin, Science 295 (2002) 1503–1506.
[11] F.P. Zamborini, M.C. Leopold, J.F. Hicks, P.J. Kulesza, M.A. Malik, R.W. Murray, J. Am. Chem. Soc. 124 (2002) 8958–8964.
[12] T. Vossmeyer, B. Guse, I. Besnard, R.E. Bauer, K. Mullen, A. Yasuda, Adv. Mater. 14 (2002) 238–242.
[13] G. Schmid, G.L. Hornyak, Curr. Opin. Solid State Mater. Sci. 2 (1997) 204–212.
[14] B. Neiman, E. Grushka, O. Lev, Anal. Chem. 73 (2001) 5220–5227.
[15] R. Griffith, K.C. Grabar, K.J. Allison, R.M. Bright, J.A. Davis, A.P. Guthrie, M.B. Hommer, M.A. Jackson, P.C. Smith, D.G. Walter, M.J. Natan, Science 267 (1995) 1629–1632.
[16] D.L. Feldheim, C.D. Keating, Chem. Soc. Rev. 27 (1998) 1–12.
[17] U. Simon, Adv. Mater. 10 (1998) 1487–1492.
[18] T. Sato, H. Ahmed, D. Brown, B.F.G. Johnson, J. Appl. Phys. 82 (1997) 696–701.
[19] D. Wyrwa, N. Beyer, G. Schmid, Nano Lett. 2 (2002) 419–421.
[20] R.P. Andres, J.D. Bielefeld, J.I. Henderson, D.B. Janes, V.R. Kolagunta, C.P. Kubiak, W.J. Mahoney, R.G. Osifchin, Science 273 (1996) 1690–1693.
[21] A.C. Templeton, W.P. Wuelfing, R.W. Murray, Acc. Chem. Res. 33 (2000) 27.
[22] M. Brust, M. Walker, D. Bethell, D.J. Schiffrin, R. Whyman, J. Chem. Soc., Chem. Commun. (1994).
[23] M.J. Hostetler, R.W. Murray, Curr. Opin. Colloid Interface Sci. 2 (1997) 42.
[24] F.P. Zamborini, J.F. Hicks, R.W. Murray, J. Am. Chem. Soc. 122 (2000) 4514–4515.
[25] W.P. Wuelfing, F.P. Zamborini, A.C. Templeton, X. Wen, H. Yoon, R.W. Murray, Chem. Mater. 13 (2001) 87–95.
[26] A.C. Templeton, F.P. Zamborini, W.P. Wuelfing, R.W. Murray, Langmuir 16 (2000) 6682–6688.
[27] J.F. Hicks, F.P. Zamborini, R.W. Murray, J. Phys. Chem. B 106 (2002) 7751–7757.
[28] J.F. Hicks, F.P. Zamborini, A.J. Osisek, R.W. Murray, J. Am. Chem. Soc. 123 (2001) 7048–7053.
[29] J.F. Smalley, S.W. Feldberg, C.E.D. Chidsey, M.R. Linford, M.D. Newton, Y.-P. Liu, J. Phys. Chem. 99 (1995) 13141.
[30] K. Weber, S. Creager, J. Phys. Chem. B 101 (1997) 8286–8291.
[31] C.E.D. Chidsey, Science 251 (1991) 919–922.
[32] R.E. Holmlin, R. Haag, M.L. Chabinyc, R.F. Ismagilov, A.E. Cohen, A. Terfort, M.A. Rampi, G.M. Whitesides, J. Am. Chem. Soc. (2001).
[33] R.E. Holmlin, R.F. Ismagilov, R. Haag, V. Mujica, M.A. Ratner, M.A. Rampi, G.M. Whitesides, Angew. Chem. Int. Ed. 40 (2001) 2316–2320.
[34] D.J. Wold, C.D. Frisbie, J. Am. Chem. Soc. 123 (2001) 5549–5556.
[35] W.P. Wuelfing, S.J. Green, J.J. Pietron, D.E. Cliffel, R.W. Murray, J. Am. Chem. Soc. 122 (2000) 11465–11472.
[36] R.H. Terrill, T.A. Postlethwaite, C.-C. Chen, C.-D. Poon, A. Terzis, A. Chen, J.E. Hutchison, M.R. Clark, G. Wignall, J.D. Londono, R. Superfine, M. Falvo, C.S. Johnson, E.T. Samulski, R.W. Murray, J. Am. Chem. Soc. 117 (1995) 12537–12548.
[37] K. Slowinski, H.K.Y. Fong, M. Majda, J. Am. Chem. Soc. 121 (1999) 7257–7261.
[38] W.P. Wuelfing, R.W. Murray, J. Phys. Chem. B 106 (2002) 3139–3145.
[39] S. Chen, R.S. Ingram, M.J. Hostetler, J.J. Pietron, R.W. Murray, T.G. Schaaff, J.T. Khoury, M.M. Alvarez, R.L. Whetten, Science 280 (1998) 2098–2101.
[40] R.A. Marcus, N. Sutin, Biochim. Biophys. Acta 811 (1985) 265–322.
[41] R.A. Marcus, Angew. Chem. Int. Ed. 32 (1993) 1111–1121.
[42] M.D. Newton, Chem. Rev. 91 (1991) 767–792.
[43] F.L. Leibowitz, W. Zheng, M.M. Maye, C.-J. Zhong, Anal. Chem. 71 (1999) 5076–5083.

[44] D. Bethell, M. Brust, D.J. Schiffrin, C. Kiely, J. Electroanal. Chem. 409 (1996) 137–143.
[45] M.D. Musick, C.D. Keating, M.H. Keefe, M.J. Natan, Chem. Mater. 9 (1997) 1499–1501.
[46] N. Fishelson, I. Shkrob, O. Lev, J. Gun, A.D. Modestov, Langmuir 17 (2001) 403–412.
[47] M.L. Sauthier, R.L. Carroll, C.B. Gorman, S. Franzen, Langmuir 18 (2002) 1825–1830.
[48] E.W.L. Chan, L. Yu, Langmuir 18 (2002) 311–313.
[49] F. Auer, M. Scotti, A. Ulman, R. Jordan, B. Sellergren, J. Garno, G.-Y. Liu, Langmuir 16 (2000) 7554–7557.
[50] Y. Liu, Y. Wang, R.O. Claus, Chem. Phys. Lett. 298 (1998) 315–319.
[51] D.L. Feldheim, K.C. Grabar, M.J. Natan, T.E. Mallouk, J. Am. Chem. Soc. 118 (1996) 7640–7641.
[52] J.F. Hicks, Y.-S. Shon, R.W. Murray, Langmuir 18 (2002) 2288–2294.
[53] S. Mann, W. Shenton, M. Li, S. Connolly, D. Fitzmaurice, Adv. Mater. 12 (2000) 147–150.
[54] A.P. Alivisatos, K.P. Johnsson, X. Peng, T.E. Wilson, C.J. Loweth, M.P. Bruchez Jr., P.G. Schultz, Nature 382 (1996) 609–611.
[55] S.-J. Park, A.A. Lazarides, C.A. Mirkin, P.W. Brazis, C.R. Kannewurf, R.L. Letsinger, Angew. Chem. Int. Ed. 39 (2000) 3845–3848.
[56] C.A. Mirkin, R.L. Letsinger, R.C. Mucic, J.J. Storhoff, Nature 382 (1996) 607–609.
[57] M. Brust, D. Bethell, D.J. Schiffrin, C. Kiely, Adv. Mater. 7 (1995) 795–797.
[58] J.P. Novak, D.L. Feldheim, J. Am. Chem. Soc. 122 (2000) 3979–3980.
[59] M. Brust, C.J. Kiely, D. Bethell, D.J. Schiffrin, J. Am. Chem. Soc. 120 (1998) 12367–12368.
[60] J. Liu, J. Alvarez, W. Ong, A.E. Kaifer, Nano Lett. 1 (2001) 57–60.
[61] M.D. Musick, C.D. Keating, L.A. Lyon, S.L. Botsko, D.J. Pena, W.D. Holliway, T.M. McEvoy, J.N. Richardson, M.J. Natan, Chem. Mater. 12 (2000) 2869–2881.
[62] M.M. Maye, J. Luo, L. Han, C.-J. Zhong, Nano Lett. 1 (2001) 575–579.
[63] J. Lohau, F.G. Dumpich, E.F. Wassermann, M. Winter, M.T. Reetz, J. Vac. Sci. Technol. B 16 (1998) 77–79.
[64] M.H.V. Werts, M. Lambert, J.-P. Bourgoin, M. Brust, Nano Lett. 2 (2002) 43–47.
[65] M.B. Ali, T. Ondarcuhu, M. Brust, C. Joachim, Langmuir 18 (2002) 872–876.
[66] T.R. Ramachandran, C. Baur, A. Bugacov, A. Madhukar, B.E. Koel, A.A.G. Requicha, C. Gazen, Nanotechnology 9 (1998) 237–245.
[67] C. Baur, A. Bugacov, B.E. Koel, A. Madhukar, N. Montoya, T.R. Ramachandran, A.A.G. Requicha, R. Resch, P. Will, Nanotechnology 9 (1998) 360–364.
[68] R. Resch, C. Baur, A. Bugacov, B.E. Koel, A. Madhukar, A.A.G. Requicha, P. Will, Langmuir 14 (1998) 6613–6616.
[69] R. Resch, C. Baur, A. Bugacov, B.E. Koel, P.M. Echternach, A. Madhukar, N. Montoya, A.A.G. Requicha, P. Will, J. Phys. Chem. B 103 (1999) 3647–3650.
[70] R. Resch, D. Lewis, S. Meltzer, N. Montoya, B.E. Koel, A. Madhukar, A.A.G. Requicha, P. Will, Ultramicroscopy 82 (2000) 135–139.
[71] M. Rolandi, K. Scott, E.G. Wilson, F.C. Meldrum, J. Appl. Phys. 89 (2001) 1588–1595.
[72] W. Yang, M. Chen, W. Knoll, H. Deng, Langmuir 18 (2002) 4124–4130.
[73] M.J. Hostetler, A.C. Templeton, R.W. Murray, Langmuir 15 (1999) 3782.
[74] M.J. Hostetler, J.E. Wingate, C.-J. Zhong, J.E. Harris, R.W. Vachet, M.R. Clark, J.D. Londono, S.J. Green, J.J. Stokes, G.D. Wignall, G.L. Glish, M.D. Porter, N.D. Evans, R.W. Murray, Langmuir 14 (1998) 17–30.
[75] Y. Xia, G.M. Whitesides, Angew. Chem. Int. Ed. 37 (1998) 550–575.
[76] C.A. Goss, D.H. Charych, M. Majda, Anal. Chem. 63 (1991) 85–88.
[77] J.F. Hicks, University of North Carolina, unpublished results.
[78] M.D. Porter, T.B. Bright, D.L. Allara, C.E.D. Chidsey, J. Am. Chem. Soc. 109 (1987) 3559–3568.
[79] C.E.D. Chidsey, D.N. Loiacono, Langmuir 6 (1990) 682–691.
[80] R.W. Murray, in: R.W. Murray (Ed.), Molecular Design of Electrode Surfaces, Wiley, New York, 1992.
[81] G.-Y. Liu, S. Xu, Y. Qian, Acc. Chem. Res. 33 (2000) 457–466.
[82] F.P. Zamborini, R.M. Crooks, J. Am. Chem. Soc. 120 (1998) 9700–9701.
[83] R.D. Piner, J. Zhu, F. Xu, S. Hong, C.A. Mirkin, Science 283 (1999) 661–663.
[84] R.L. McCarley, T.E.A. Irene, R.W. Murray, J. Electrochem. Soc. 137 (1990) 1485–1490.
[85] D.J. Diaz, J.E. Hudson, G.D. Storrier, H.D. Abruna, N. Sundararajan, C.K. Ober, Langmuir 17 (2001) 5932–5938.
[86] D.C. Tully, K. Wilder, J.M.J. Frechet, A.R. Trimble, C.F. Quate, Adv. Mater. 11 (1999) 314–318.
[87] Y.-R. Ma, C. Yu, Y.-D. Yao, Y. Liou, S.-F. Lee, Phys. Rev. B 64 (2001) 1953241–1953245.

Francis P. Zamborini received his BS in chemistry from Carthage College (Kenosha, WI) in 1993 and a PhD in chemistry from Texas A&M University (College Station, TX) in 1998. Under the direction of Richard M. Crooks, his doctoral research focused on the use of self-assembled monolayers for corrosion passivation and nanolithography as studied by scanning probe microscopy, electrochemistry, and surface spectroscopy. He studied under Royce W. Murray at the University of North Carolina, Chapel Hill as a Postdoctoral Research Associate from 1998 to 2001, focusing on assembly, electron transport, and chemical sensing properties of gold nanoparticles. Frank's current research interests are in one-dimensional assembly of metal nanoparticles, surface forces, and nanosensors. He is a member of the ElectroOptics Research Institute and Nanotechnology Center at the University of Louisville.